Progress In Electromagnetics Research, Vol. 108, 323–341, 2010

ANALYSIS OF PERPENDICULAR CROSSING DIELECTRIC WAVEGUIDES WITH VARIOUS TYPICAL INDEX CONTRASTS AND INTERSECTION PROFILES

H.-W. Chang and Y.-H. Wu

Institute of Electro-optical Engineering
Department of Photonics
National Sun Yat-sen University
Kaohsiung 80424, Taiwan

Abstract—We present a rigorous 2D numerical study of the transmission, reflection and crosstalk coefficients of the perpendicular, identical dielectric crossing waveguide with various core-cladding index contrasts for both TE and TM polarizations. Our method is based on a hybrid frequency-domain finite-difference (FD-FD) technique computed with the cross-symmetry model. By varying the intersection profile, such as the circular, filleted, tapered and elliptical shapes, we achieve, even for a large 3.5 to 1.5 index ratio, a low 0.25 dB insertion loss, a nontrivial reduction over the straight direct crossing case.

1. INTRODUCTION

High density photonic interconnecting networks require a more complex design of planar lightwave circuits than its predecessors. Therefore, the fabrication of the dielectric waveguide crossings with low insertion loss and low crosstalk is of great importance [1–3]. There are many publications [4–9] regarding dielectric waveguide crossings, specifically those implemented on silicon-on-insulator (SOI) chips [10–12]. In order to enhance the transmission and to lower the crosstalk [13], there are many different intersection profiles of the direct crossing structure, including the multimode interference (MMI) structure [14], resonant cavity and elliptical or parabolic mode expanders. However, it is difficult to analyze a four-port

Received 10 August 2010, Accepted 16 September 2010, Scheduled 24 September 2010
Corresponding author: H.-W. Chang (hchang@faculty.nsysu.edu.tw).

waveguide crossing coupled tightly with the vertical and horizontal propagating waves in the vicinity of the intersection. For example, BPM [15] cannot compute the wave fields propagating in the upward and downward directions of crossing waveguide. Furthermore, the more complex intersection profiles make the analysis difficult for the rigorous methods such as the quadridirectional mode matching methods [16, 17] and the coupled transverse-mode integral equation CTMIE methods [18, 19]. These mode-based methods adopt PECAM (Perfect Electric Conductor approximation method), which confines the wave fields to horizontal propagation. Although it is possible to modify the mode matching method to obtain a quadridirectional eigenmode expansion scheme [20–22] for crossing waveguides, this highly accurate method is difficult to implement for an arbitrary crossing profile. The general PML boundary conditions are often combined with PECAM schemes but are not suitable for the waveguide crossing due to the strong evanescent waves in the cladding region of guiding modes [23–25].

We observed that there were two different results on the elliptical mode expanders with different short to long axis ratios. The first model [7], which is based on a 3D FDTD method [26–32], claimed the insertion loss and crosstalk were $< 0.1\,\mathrm{dB}$ and $< -25\,\mathrm{dB}$, respectively, at $\lambda = 1.51$–$1.57\,\mu\mathrm{m}$ for an elliptical region with respective short and long axes of $1.5\,\mu\mathrm{m}$ and $7.2\,\mu\mathrm{m}$. However, the second model [10] for an elliptical region with short and long axes of $2.5\,\mu\mathrm{m}$ and $6.0\,\mu\mathrm{m}$, at $\lambda = 1.55\,\mu\mathrm{m}$ demonstrated a transmission of 32%. The different crossing profiles lead to contrasting transmission performances, would confound the readers.

This is an interesting problem regarding the design of intersection profile parameters to improve the transmission, and reduce reflection and crosstalk of waveguide crossings. There are many excellent analytic or semi-analytical methods for studying complex devices, including but not limited to analytic continuity method [33], finite-element boundary integral equation method [34], coupled mode theory [35], combined-field integral equation [36] and etc. These analytic or semi-analytical methods are difficult to modify for our proposed crossing structures. On the other hand, the most popularly used, FDTD method and its variants are not suited for modeling complex waveguide devices with narrow-band signal. The less popular FD-FD method and its variants [37–41], due to their need for solving large sparse linear equations, are more accurate in frequency domain applications.

In this paper, we apply a rigorous 2D, hybrid FD-FD method to study the design of an optimal crossing waveguide. Our hybrid

FD-FD method employs an accurate, layer-mode based, transparent boundary conditions (LM-TBC) [38] which absorb/transmit guided modes, discretized radiation modes and even the evanescent modes in both crossing waveguides.

Although 3D calculations will provide closer results to a real system, or predicting cross-talk values for the real world, we will now focus on simulating ideal 2D crossing waveguides with our 2D, full-wave, hybrid FD-FD method [41]. Let us try to characterize the right angle crossing waveguide as shown in Fig. 1(a). By applying the cross (X) symmetric model, which is more stable and precise than the plus ($+$) symmetric one [41], as shown in Fig. 1(b), we can simplify the computational domain with transparent boundary conditions (TBC) on all four borderlines to one quarter of the original region with only one borderline needed. The calculation of transmission (or insertion loss), reflection loss and crosstalk is represented as a function of the waveguide core thickness and core-cladding indices. We study different modified intersection profiles and design their parameters to improve the transmission and crosstalk performance of the waveguide crossing.

2. THE DESIGN OF THE INTERSECTION PROFILE

2.1. The Simple Direct Crossing

From Fig. 1(a), we let D be the core width of both horizontal and vertical dielectric waveguides. λ is the wavelength of the incident field. We also assume the fundamental mode is coming from the left side. In the cross symmetry model shown in Fig. 1(b), we have two $\pm 45^\circ$ symmetric lines perpendicular to each other. We choose the left quarter as our computational domain. For this cross symmetry model there are four symmetry condition pairs denoted by the subscript of MM, EM, ME and EE. The first letter represents the PEC/PMC wall (EW/MW for short) on the upper right border and the second letter for the lower right boundary. This model allows us to reduce the original/full problem to four sub-problems, which individually require less computing resources [41].

The FD-FD formulations of the two-dimensional Helmholtz equation for TE and TM modes are listed as follows:

$$\begin{aligned} c_u^e u_u + c_d^e u_d + c_\ell^e u_\ell + c_r^e u_r + c_c^e u_c = 0, \\ c_u^h u_u + c_d^h u_d + c_\ell^h u_\ell + c_r^h u_r + c_c^h u_c = 0, \end{aligned} \tag{1}$$

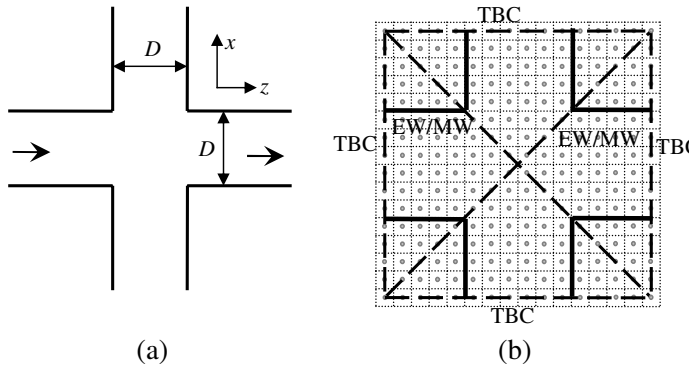

Figure 1. (a) The open perpendicular dielectric waveguide crossing. (b) The two-fold symmetry of this crossing produces equivalent boundary conditions on the two perpendicular, diagonal dotted lines. Our FD-FD simulation is only performed on the left quarter with the cross symmetry model [41-Fig. 6].

where the coefficients are given by:

$$\begin{aligned}
&c_u^e = c_d^e = 1/\Delta x^2, \quad c_\ell^e = c_r^e = 1/\Delta z^2, \\
&c_c^e = \overline{n_c^2} k_0^2 - (c_u^e + c_d^e + c_\ell^e + c_r^e), \\
&c_u^h = \frac{\bar{1}}{n_u^2}\frac{1}{\Delta x^2},\ c_d^h = \frac{\bar{1}}{n_d^2}\frac{1}{\Delta x^2},\ c_\ell^h = \frac{\bar{1}}{n_\ell^2}\frac{1}{\Delta z^2},\ c_r^h = \frac{\bar{1}}{n_r^2}\frac{1}{\Delta z^2}, \\
&c_c^h = k_0^2 - \left(c_u^h + c_d^h + c_\ell^h + c_r^h\right).
\end{aligned} \tag{2}$$

Here k_0 is the wave number in vacuum. $\overline{n_c^2}$ is given by the average of $n^2(x,z)$ centered around the field point u_c over a grid cell area $\Delta x \cdot \Delta z$ for TE case. TM case requires the average $\overline{1/n_p^2}$, which is defined as a real average of $1/n_p^2(x,z)$ centered at the field point u_p. When $p = u, d, \ell, r$, the center of the integration point is respectively located half a grid up, down, left and right from u_c. TE and TM FD coefficients are identical except for those points laid within one grid, away from boundaries between two materials. These material dependent FD coefficients are defined differently for TE and TM polarizations, for a good reason. For a small core-cladding index contrast, TE average ($\overline{n^2}$) and TM ($\overline{1/n^2}$) average are about the same. But when the index contrast is large, the TM average of $1/n^2(x,z)$ will be different from 1 over the average of $n^2(x,z)$. This is explained in further detail in our first crossing paper Ref. [41].

By combining the quarter-fields of all four cases from different symmetric conditions, we obtain the sum of all four simulations

which produces just one incident field coming from the left waveguide. For a detailed explanation, see [41-Fig. 9]. If we denote the reflection coefficients of Fig. (1b)'s left-quarter waveguide as R_{MM}, R_{EE}, R_{EM}, R_{ME}, we obtain the reflection, top and bottom cross, and transmission coefficients of the dielectric waveguide crossing in Fig. (1a) as the following equation:

$$\begin{aligned} R &= \frac{R_{\mathrm{MM}} + R_{\mathrm{EE}} + R_{\mathrm{EM}} + R_{\mathrm{ME}}}{4}, \\ C_{\mathrm{top}} &= \frac{R_{\mathrm{MM}} - R_{\mathrm{EE}} - R_{\mathrm{EM}} + R_{\mathrm{ME}}}{4}, \\ C_{\mathrm{bot}} &= \frac{R_{\mathrm{MM}} - R_{\mathrm{EE}} + R_{\mathrm{EM}} - R_{\mathrm{ME}}}{4}, \\ T &= \frac{R_{\mathrm{MM}} + R_{\mathrm{EE}} - R_{\mathrm{EM}} - R_{\mathrm{ME}}}{4}. \end{aligned} \tag{3}$$

Here R and T are the reflection and transmission coefficients of the perpendicular crossing waveguide. C_{top} and C_{bot} are the top and bottom cross coupling coefficients, which are identical in magnitude in this case. The four coefficient vectors are ratios between the scattered mode amplitudes and the fundamental incident mode amplitude. The reflected, transmitted and cross coupling power coefficients are computed as squared, absolute values times the ratio between the real parts of the scattered mode propagation constants and the fundamental mode propagation constant [42].

2.2. Type of Intersection Profiles

Figure 2 shows four types of dielectric waveguide crossings with different intersection profile variations. These should cover most similar profile variations with identical horizontal and vertical waveguides which is the fundamental assumption in this paper.

We define, r_c, as the ratio between the radius for the circular profile (Fig. 2(a)) and the core thickness ($W_{\mathrm{cor}} = D$) of the slab waveguide:

$$r_c = \frac{\sqrt{2}R_c}{W_{\mathrm{cor}}}, \tag{4}$$

At its minimum value, $r_c = 1$, we have a textbook case of straight direct crossing. The circular model provides a ball lens function, where the circular intersection helps confine the field in the core for the SOI. Next, for the filleted shape (Fig. 2(b)), we define r_f as the ratio between of the profile radius and the core thickness of the slab waveguide:

$$r_f = \frac{2R_f}{W_{\mathrm{cor}}}. \tag{5}$$

In this filleted model, we predict an improved field transfer through the adiabatic profile. This effect could result in better mode transmission.

When direct crossings of two perpendicular waveguides suffer from large insertion losses or unwanted mode conversion, the tapered waveguide can be used to smooth the mode transitions between waveguides of different widths. An illustration of a tapered crossing, as seen in Fig. 2(c), has a tapered slope of:

$$r_{\text{taper}} = \frac{(2H - W_{\text{cor}})}{2L}, \tag{6}$$

where H is half the height of the end of the taper and L is the tapered length. The example used in Fig. 2(c) has a positive tapered slope. The original waveguide width D is gradually and linearly increased/decreased to the tapered waveguide width of $2H$. When $2H < W_{\text{cor}}$, the ratio r_{taper} is negative. This indicates a narrowing tapered width. By combining the lens-focusing (2a) and tapering (2c) properties, we have a final design, shown in Fig. 2(d), where the tapered regions are partially shaped like ellipses. In this case, the functions of

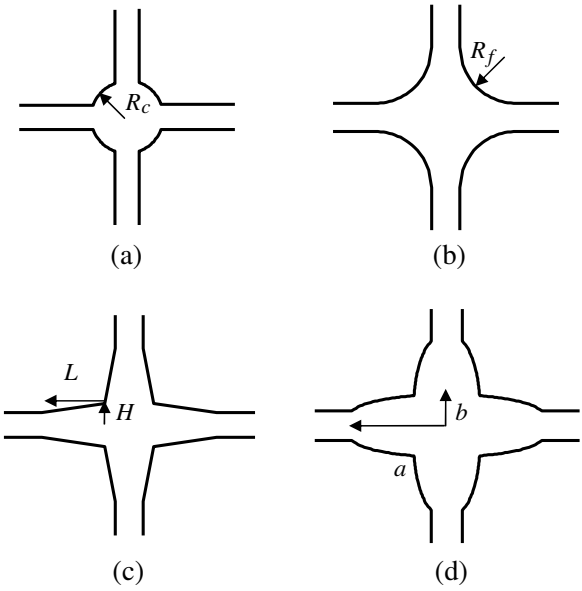

Figure 2. The different intersection types for a perpendicular crossing waveguide. (a) The crossing with a circular shape. (b) The crossing with a filleted shape. (c) The crossing with a tapered shape. (d) The crossing with an elliptical shape.

the horizontal and vertical elliptical shapes are:

$$\begin{aligned} \frac{z^2}{a^2} + \frac{x^2}{b^2} &= 1, \quad \text{(horizontal)} \\ \frac{z^2}{b^2} + \frac{x^2}{a^2} &= 1, \quad \text{(vertical)} \end{aligned} \tag{7}$$

where a and b are, respectively, the long and short axis of the ellipse. Results from our simulations indicate that this model has the benefit of a focusing lens, which boosts the fundamental mode transmission coefficients. Within these models, Fig. 2(d) provides the best design for achieving minimal insertion losses.

3. RESULTS AND DISCUSSION

We present the numerical results on field distributions and power reflection, transmission and crosstalk of dielectric crossing waveguides for the three index contrast ranges currently commercially available. These contrasts vary from low to high with 3.45/3.38 contrast, an intermediate 2.5/1.5 contrast, to a high 3.45/1.5 contrast. Using simple direct crossings as a reference, our results include the analysis for four intersection profiles, three index contrasts and for both TE and TM polarizations.

3.1. Two-dimensional Field Plots

Field distributions of five types of crossing waveguides are shown in Figs. 3 to 7 with the real parts on the upper halves and the imaginary parts on the bottom halves. The SOI waveguides have a high index contrast with $n_{cor} = 3.45$ and $n_{cld} = 1.5$. For all Figs. 3 to 7, the incident wavelength is set at 1.55 µm with the dielectric slab waveguides width at 0.6 µm. These slab waveguides each have two even and one odd guiding modes. We see in Fig. 3 that the EM fields in the direct crossing are mostly confined in the core. For this case, the fundamental mode transmission coefficients for TE and TM cases are 86% and 77%, respectively. Total crossing power coefficients are 5% and 11% for TE and TM polarizations, of which, more than 95% is radiation power. The total reflected powers are less than 1% in both polarizations and are also dominated by radiation energy. Figs. 4 to 7 provide us with the field distributions of circular, filleted, tapered and elliptical intersection profiles respectively. In Figs. 4 and 5, we see stronger reflection and crosstalk power in both the circular and filleted intersections, resulting in a reduced fundamental mode transmission coefficient less than 66% in both profiles and both polarizations. For

the tapered profile, the transmission coefficient is calculated to be 86% in the TE case which approximates that of the direct crossing. Meanwhile the transmission coefficient reaches 81% in the TM case which is an improvement over the direct crossing. The most dramatic improvement for waveguides of the same dimensions, is that of Fig. 7's profile, where the fundamental mode transmission coefficients are 93% and 92% for the TE and TM cases.

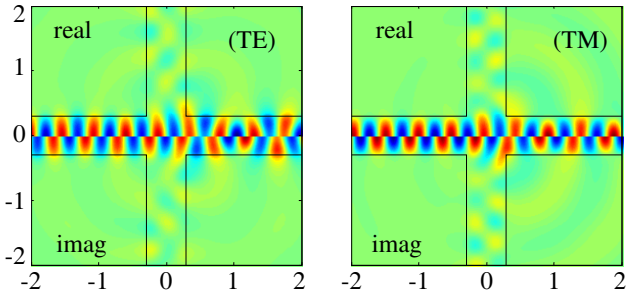

Figure 3. The TE ($E_y(x, z)$) and TM ($H_y(x, z)$) field distributions of an open perpendicular dielectric crossing waveguide in the vicinity of the waveguide junction. These complex EM fields are shown with the real part on the upper halves and the imaginary part on the bottom halves which clearly show the dominance of the forward propagating fundamental mode. The units on both horizontal and vertical axes are in microns.

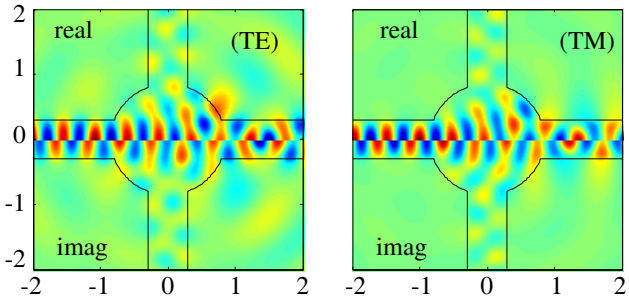

Figure 4. The circular intersection profile for TE and TM field distributions of an open dielectric crossing waveguide. We can see the presence of higher-order guide mode in the transmitted waveguide due to stronger mode conversion in the waveguide junction. The units on both horizontal and vertical axes are in microns.

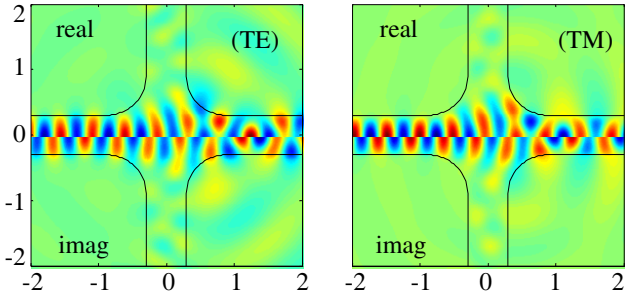

Figure 5. The filleted intersection profile.

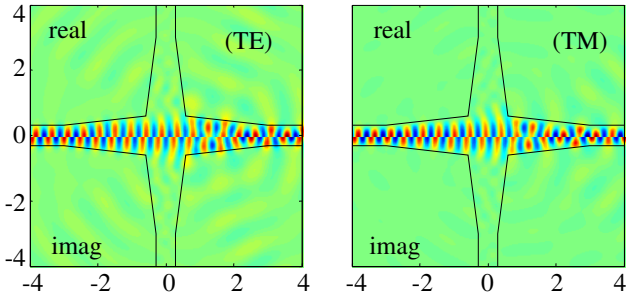

Figure 6. The taper intersection profile.

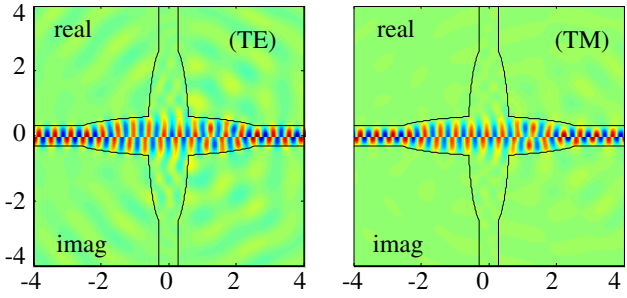

Figure 7. The elliptical intersection profile, which possesses the highest fundamental mode transmission efficiency in all Figs. 3 to 7.

3.2. Power Coefficients of Direct Crossing

With the hybrid FD-FD simulation of crossing waveguides, we are able to obtain mode-to-mode, through and cross coupling coefficients, as well as reflection coefficients, as function of wavelength and waveguide structure parameters. The goal of designing a good waveguide crossing is to fabricate a crossing profile that minimizes insertion loss, ensuring

maximized fundamental mode transmission efficiency. This is to achieved by lowering reflected and cross coupling powers. However, a high total transmitted power design does not always guarantee the highest fundamental mode power transmission coefficient, due to potential transmission of higher-order mode powers in the transmitted wave fields. In order to construct an ideal waveguide crossing profile, we should first study scattered power coefficients of the generic direct waveguide crossing. These standard direct crossing curves will be used to aide the designing of more complicated crossing profiles.

Figures 8 and 9 plot the total TE/TM transmission power coefficients for identical, perpendicular dielectric waveguide crossings, as function of waveguide core thickness. We list three different core-cladding index contrasts, where n_r is the core cladding index ratio with the actual indices shown in parenthesis. We show combined power transmission coefficient, P_t, including higher-order guided, and all radiation modes (Fig. 8(a), Fig. 9(a)) as well as the power coefficient, P_{t1}, for the fundamental mode only (Fig. 8(b), Fig. 9(b)). For both polarizations we observe higher values with the small core thickness. This would suggest shaping the design towards small W_{cor} to achieve low insertion losses. The drawbacks in such designs for dielectric

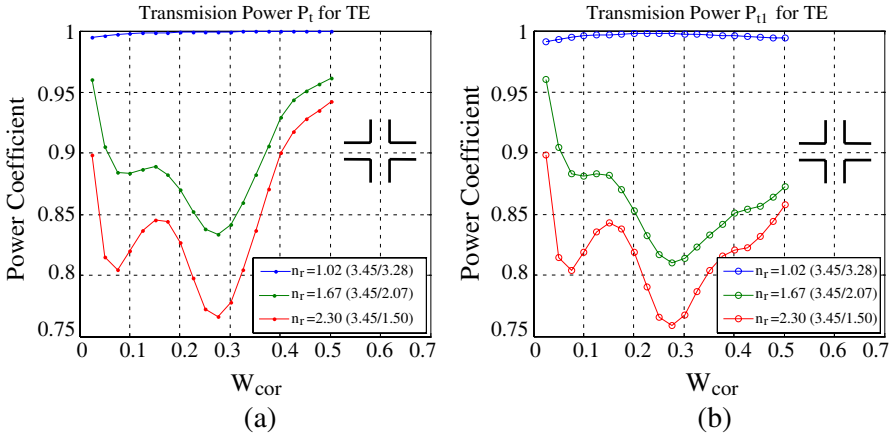

Figure 8. The TE transmission power coefficient reference curve for identical, perpendicular dielectric waveguide crossings. We list three different core-cladding index contrasts, where n_r is the core cladding index ratio with the actual indices shown in the parenthesis. (a) Combines the fundamental, higher order guided, and all radiation modes. (b) Fundamental mode only. The unit on the horizontal axis is in microns.

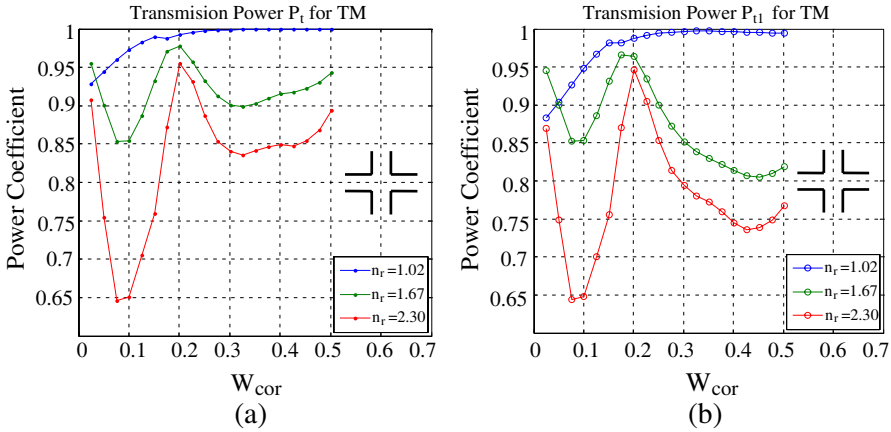

Figure 9. The TM transmission power coefficient reference curve for identical, perpendicular dielectric waveguide crossings. We list three different core-cladding index contrasts, as in Fig. 8. (a) Combines the fundamental, higher order guided, and all radiation modes. (b) Fundamental mode only. The unit on the horizontal axis is in microns.

waveguides with small core widths are that fields are not confined in the cores; rather, they extend far into the cladding. Our simulation results also show that for normal and large waveguide core widths, it is hard to achieve high P_{t1} in direct perpendicular crossings when the core-cladding index contrast is large.

3.3. Power Coefficients of Crossing with a Circular Shape

From here on we focus only on the fundamental mode power transmission coefficients P_{t1} for the remaining four crossing profiles. The results for the circular shaped crossing waveguides are shown in Fig. 10 where P_{t1} is plotted against r_c (Eq. (4) profile parameter) with a fixed core thickness $W_{\text{cor}} = 0.2\,\mu\text{m}$. We see from Fig. 10 that except for the low n_r case, the circular shape design is ineffective in the TE mode. However, it does improve the TM fundamental mode power transmission coefficients for larger n_r ratios at ideal, select ranges R_c.

3.4. Power Coefficients of Crossing with a Filleted Shape

The results for the filleted shaped crossing waveguides are shown in Fig. 11 where P_{t1} is plotted against r_f (Eq. (5) profile parameter) with a fixed core thickness $W_{\text{cor}} = 0.2\,\mu\text{m}$. As with the previous shape, the filleted shape is ineffective for TE polarization. But for

TM polarization the filleted shape can significantly improve the power transmission in the high index contrast case with a r_f value slightly greater than one.

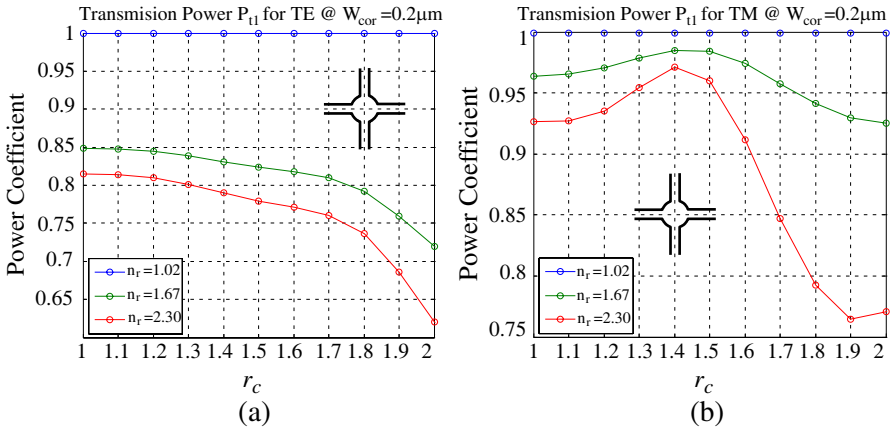

Figure 10. The fundamental mode power transmission coefficients for three different core-cladding index contrasts in a circular profile crossing waveguide. The horizontal axis, r_c, is the Fig. 2(a) dimensionless profile parameter defined in Eq. (4). (a) TE polarization. (b) TM polarization.

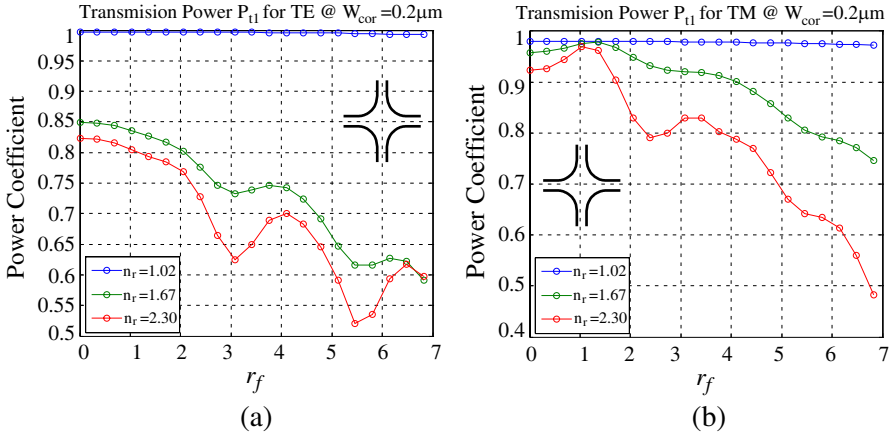

Figure 11. The fundamental mode power transmission coefficients for three different core-cladding index contrasts in a filleted shape profile crossing waveguide. The horizontal axis, r_f, is the Fig. 2(b) profile parameter defined in Eq. (5). (a) TE polarization. (b) TM polarization. The horizontal axis is dimensionless.

3.5. Power Coefficients of Crossing with a Tapered Shape

With the waveguide core thickness fixed at $W_{\text{cor}} = 0.4\,\mu\text{m}$ and a fixed tapered length of $4\,\mu\text{m}$ so that the position of the taper starts at $z = -4\,\mu\text{m}$ for the left incident waveguide, the results for the tapered crossing waveguides are shown in Fig. 12, where P_{t1} is plotted against r_{taper} (See Eq. (6)). These plots are for both negative and positive r_{taper}. We see that the tapered shape improves P_{t1} over the direct crossing ($r_{\text{taper}} = 1$) for both TE and TM modes. However, this is not the optimum profile design when compared with the elliptical profile.

3.6. Power Coefficients of Crossing with an Elliptical Shape

The final crossing design in this paper is the elliptical profile. We examine this case with a waveguide core thickness fixed at $W_{\text{cor}} = 0.4\,\mu\text{m}$ and a long axis fixed at $a = 3\,\mu\text{m}$. The short axis is the changing variable starting from $b = 0.2\,\mu\text{m}$ to $b = 1.5\,\mu\text{m}$, during which, the assumed wavelength is $\lambda = 1.5\,\mu\text{m}$. In Fig. 13, we plot P_{t1} against the b/a ratio for the three index contrasts. The elliptical shape improves the direct crossing efficiency for both TE and TM modes at select small b/a ratios. But when this ratio is larger than 0.3, the insertion loss increases rapidly. Finally we notice that amongst all crossing profiles,

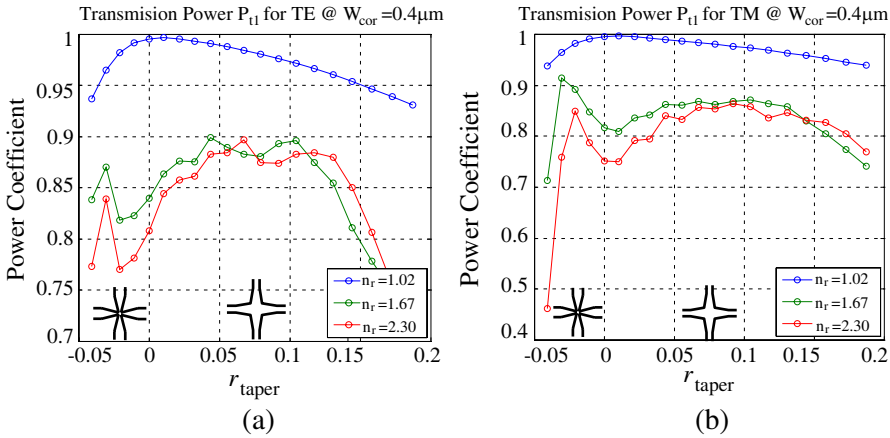

Figure 12. The fundamental mode power transmission coefficients for three different core-cladding index contrasts in a tapered profile crossing waveguide. The horizontal axis, r_{taper}, is the Fig. 2(c) dimensionless profile parameter defined in Eq. (6). (a) TE polarization. (b) TM polarization.

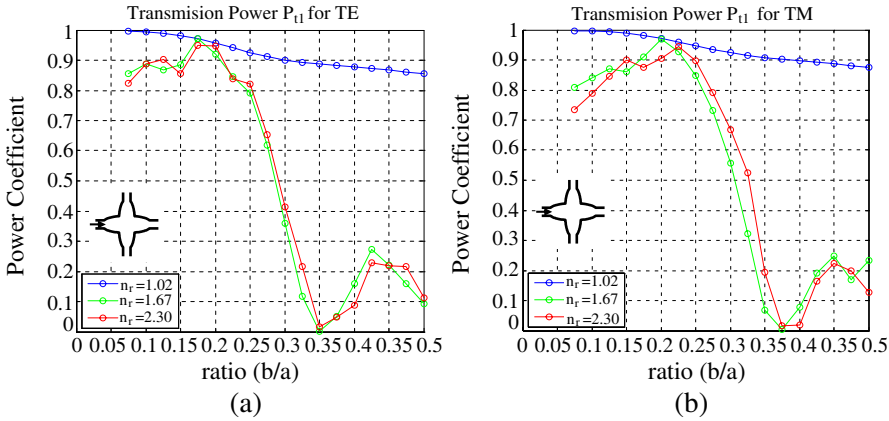

Figure 13. The fundamental mode power transmission coefficients for three different core-cladding index contrasts within an elliptical shaped crossing waveguide. This is the only design that achieves low insertion loss for both (a) TE polarization and (b) TM polarizations.

the elliptical shape is the only design that can achieve a low 0.25 dB insertion loss, even for the large 3.5 to 1.5 index ratios, for both TE and TM polarizations. This is a nontrivial reduction over the straight direct crossing case.

4. DISCUSSION: TWO-D VERSUS THREE-D SIMULATION

In this paper, we apply a rigorous 2D, hybrid FD-FD method to study the design of an optimal crossing waveguide. As far as we know, a full 3D, hybrid FD-FD simulation for a real crossing waveguide design is beyond our capability. In a 2D (z, x) case, six component EM fields can be exactly decomposed into a three component TE $(E_y,\ H_x, H_z)$ and three component TM $(H_y,\ E_x, E_z)$ case. In each case the in-plane x-z components can be derived from the out of the plane component. Thus, we can treat all 2D problems by solving a scalar Helmholtz equation. There are however no pure TE or TM modes in a 3D dielectric waveguide device where all six-components are simultaneously presented. As a result, to conduct full-wave 3D optical device simulating, it is only possible to do it by the FD-TD method where numerical time stepping is performed without inversion of a linear equation. The drawback of FD-TD method is that accurate and stable implementation of absorbing or transparent boundary conditions (ABC or TBC) in the 3D complex structure is very difficult except with padding of large PML regions on the computational boundaries.

A full 3D FD-FD implantation using multiple field components is still under development. And even with a working 3D numerical algorithm, solving a linear equation with up to a billion variables is totally unpractical with today's hardware. Hence, 2D calculations have their own virtues in predicting cross-talk values for the real world. In this case, the 2D situation makes use of some sort of approximation to neglect both the third dimension and the polarization effects. The easiest method is called the effective index method. It tries to correct 3D and polarization effects by an index adjustment. The effective index method works fine when index contrasts are very small. When we apply the effective index approximation to high index-contrast cases, such as a photonics wire [43], the difference between n_{eff} and core index is quite significant and polarization dependent. For instance, at the 1D single-mode threshold, for Si thickness of 260 nm in SOI the core index is 3.5. To conduct 2D simulation of this 3D device one may have to use a TE $n_{\text{eff}}^{\text{TE}} = 3.0$ and a TM $n_{\text{eff}}^{\text{TM}} = 2.4$. That would make conclusions for silicon photonic wire quite off range.

5. CONCLUSION

We applied a 2D hybrid frequency-domain finite-difference method to characterize the open dielectric crossings waveguides with various refractive index contrasts in both TE and TM polarizations. We have analyzed various typical intersection profile designs for the improvement of the dielectric waveguide, fundamental-mode forward crossing coefficients. We found very limited improvement in the circular and filleted shape designs for the TE polarization while, contrarily, their TM polarization efficiencies are satisfactory.

Our best low insertion loss results are found with the elliptical shape, which seems to combine the focusing properties of a lens with the smooth mode-transition properties of a tapered waveguide. We have reached our goal of achieving a low 0.25 dB insertion loss, even for a large 3.5 to 1.5 index ratio for TM as well TE polarizations. Our numerical data is verified by crossing checking results from two symmetry models and by using even and odd N_x grids for the cross-symmetry model [41]. For each simulation, our error margin for energy conservation is verified to be within less than one percent.

ACKNOWLEDGMENT

We are grateful to the support of the National Science Council of the Republic of China under the contracts NSC98-2221-E110-012. This

work is also supported by the Ministry of Education, Taiwan, under the Aim-for-the-Top University Plan.

REFERENCES

1. Gaburro, Z., "Silicon Photonics," *Optical Interconnect*, Ch. 4, *Topics in Appl. Phys.*, Vol. 94, 121–176, 2004.
2. Pavesi, L. and G. Guillot, *Optical Interconnect*, Springer-Verlag, Berlin, Heidelberg, 2006.
3. Beausoleil, R. G., P. J. Kuekes, G. S. Snider, S.-Y. Wang, and R. S. Williams, "Nanoelectronic and nanophotonic interconnect," *Proc. IEEE*, Vol. 96, 230–247, 2008.
4. Daly, M. G., P. E. Jessop, and D. Yevick, "Crosstalk reduction in intersecting RIB waveguide," *Journal of Lightwave Technology*, Vol. 14, 1695–1698, 1996.
5. Johnson, S. G., C. Manolatou, J. D. Joannopoulos, et al., "Elimination of cross talk in waveguide intersections," *Optics Letters*, Vol. 23, 1855–1857, 1998.
6. Manolatou, C., S. G. Johnson, J. D. Joannopoulos, et al., "High-density integrated optics," *Journal of Lightwave Technology*, Vol. 17, 1682–1692, 1999.
7. Fukazawa, T., T. Hirano, F. Ohno, and T. Baba, "Low loss intersection of Si photonic wire waveguides", *Jpn. J. Appl. Phys.* Vol. 43, 646–647, 2004.
8. Liu, H., H. Tam, P. K. A. Wai, and E. Pun, "Low-loss waveguide crossing using a multimode interference structure," *Optics Communications*, Vol. 241, 99–104, 2004.
9. Jamid, H. A., M. Z. M. Khan, and M. Ameeruddin, "A compact 90° three-branch beam splitter based on resonant coupling," *Journal of Lightwave Technology*, Vol. 23, 3900–3906, 2005.
10. Bogaerts, W., P. Dumon, D. V. Thourhout, and R. Baets, "Low-loss, low-cross-talk crossings for silicon-on-insulator nanophotonic waveguides," *Optics Letters*, Vol. 32, 2801–2803, 2007.
11. Sanchis, P., J. V. Galn, A. Griol, J. Mart, M. A. Piqueras, and J. M. Perdigues, "Low-crosstalk in silicon-on insulator waveguide crossings with optimized-angle," *IEEE Photon. Technol. Lett.*, Vol. 19, 1583–1585, 2007.
12. Menzel, W. and I. Wolff, "A method for calculating the frequency-dependent properties of microstrip discontinuities," *IEEE MTT*, Vol. 25, 107–112, 1977.
13. Li, J., D. A. Fattal, and R. G. Beausoleil, "Crosstalk-free design

for the intersection of two dielectric waveguides," *Optics Express*, Vol. 17, 7717–7724, 2009.

14. Chen, H. and A. W. Poon, "Low loss multimode interference based crossings for silicon wire waveguides," *IEEE Photonics Tech. Letters*, Vol. 18, No. 21, 2260–2262, 2006.
15. Neyer, A., W. Nevenkamp, L. Thylen, and B. Lagerstrom, "A beam propagation method analysis of active and passive waveguide crossings," *Journal of Lightwave Technology*, Vol. 3, 635–642, 1985.
16. Gharib, M., E. Mehrshahi, and M. Tayarani,, "An accurate design of E-septum waveguide filters with improved stop band based on mode matching method," *Journal of Electromagnetic Waves and Applications*, Vol. 22, Nos. 14–15, 2003–2013, 2008.
17. Kusiek, A. and J. Mazur, "Analysis of scattering from arbitrary configuration of cylindrical objects using hybrid FD mode-matching method," *Progress In Electromagnetics Research*, Vol. 97, 105–127, 2009.
18. Chang, H.-W., Y.-H. Wu, S.-M. Lu, and W.-C. Cheng, "Field analysis of dielectric waveguide devices based on coupled transverse-mode integral equation — Numerical investigation," *Progress In Electromagnetics Research*, Vol. 97, 159–176, 2009.
19. Chang, H.-W. and M.-H. Sheng, "Field analysis of dielectric waveguide devices based on coupled transverse-mode integral equation — Mathematical and numerical formulations," *Progress In Electromagnetics Research*, Vol. 78, 329–347, 2008.
20. Hammer, M., "Quadridirectional eigenmode expansion scheme for 2-D modeling of wave propagation in integrated optics," *Optics Communications*, Vol. 235, 2004.
21. Hammer, M., "Hybrid analytical/numerical coupled-mode modeling of guided-wave devices," *Journal of Lightwave Technology*, Vol. 25, 2287–2298, 2007.
22. Borges, B.-H. V. and P. R. Herczfeld, "Coupled-mode analysis of highly asymmetric directional couples with periodic perturbation," *IEEE Trans. Microwave Theory Tech.*, Vol. 46, No. 3, 215–226, 1998.
23. Mittra, R. and U. Pekel, "A new look at the perfectly matched layer (PML) concept for the reflectionless absorption of electromagnetic waves," *IEEE Microwave and Guided Wave Letter*, Vol. 5, No. 3, 1995.
24. Moerloose, J. D. and M. A. Stuchly, "Behavior of Berenger's ABC for evanescent waves," *IEEE Microwave and Guided Wave Letter*,

Vol. 5, No. 10, 1995.

25. Zheng, K., W. Y. Tam, D. B. Ge, and J. D. Xu, "Uniaxial PML absorbing boundary condition for truncating the boundary of DNG metamaterials," *Progress In Electromagnetics Research Letters*, Vol. 8, 125–134, 2009.
26. Ali, M. and S. Sanyal, "FDTD analysis of rectangular waveguide in receiving mode as EMI sensors," *Progress In Electromagnetics Research B*, Vol. 17, 291–303, 2008.
27. Swillam, M. A., M. H. Bakr, and X. Li, "Full wave sensitivity analysis of guided wave structures using FDTD," *Journal of Electromagnetic Waves and Applications*, Vol. 22, No. 16, 2135–2145, 2008.
28. Khajehpour, A. and S. A. Mirtaheri, "Analysis of pyramid EM wave absorber by FDTD method and comparing with capacitance and homogenization methods," *Progress In Electromagnetics Research Letters*, Vol. 3, 123–131, 2008.
29. Sani, N. V., A. Mohammadi, A. Abdipour, and F. M. Ghannouchi, "Analysis multiport receivers using FDTD technique," *Journal of Electromagnetic Waves and Applications*, Vol. 23, Nos. 5–6, 635–643, 2009.
30. Dai, S. Y., C. M. Zhang, and Z. S. Wu, "Electromagnetic Scattering of objects above ground using MRTD/FDTD hybrid method," *Journal of Electromagnetic Waves and Applications*, Vol. 23, No. 16, 2187–2196, 2009.
31. Chatterjee, A. and R.-S. Myong, "Efficient implementation of higher-order finite volume time-domain method for electrically large scatterers," *Progress In Electromagnetics Research B*, Vol. 17, 233–254, 2009.
32. Shao, W., S.-J. Lai, and T. Z. Huang, "Compact 2-D full-wave order-marching time-domain method with a memory-reduced technique," *Progress In Electromagnetics Research Letters*, Vol. 6, 157–164, 2009.
33. Chang, H.-W. and W.-C. Cheng, "Analysis of dielectric waveguide termination with tilted facets by analytic continuity method," *Journal of Electromagnetic Waves and Applications*, Vol. 21, No. 12, 1621–1630, 2007.
34. Hua, Y., Q. Z. Liu, Y. L. Zou, and L. Sun, "A hybrid FE-BI method for electromagnetic scattering from dielectric bodies partially covered by conductors," *Journal of Electromagnetic Waves and Applications*, Vol. 22, No. 12, 423–430, 2008.
35. Liau, J.-J. N.-H. Sun, S.-C. Lin, R.-Y. Ro, J.-S. Chiang, C.-

L. Pan, and H.-W. Chang, "A new look at numerical analysis of uniform fiber Bragg gratings using coupled mode theory," *Progress In Electromagnetics Research*, Vol. 93, 385–401, 2009.

36. Fan, Z. H., D. Z. Ding, and R. S. Chen, "The efficient analysis of electromagnetic scattering from composite structures using hybrid CFIE-IEFIE," *Progress In Electromagnetics Research B*, Vol. 10, 131–143, 2009.
37. Zhao, W., H. W. Deng, and Y. J. Zhao, "Application of 4-component compact 2-D FDFD method in analysis of lossy circular metal waveguide," *Journal of Electromagnetic Waves and Applications*, Vol. 22, Nos. 17–18, 2297–2308, 2008.
38. Chang, H.-W., W.-C. Cheng, and S.-M. Lu, "Layer-mode transparent boundary condition for the hybrid FD-FD method," *Progress In Electromagnetics Research*, Vol. 94, 175–195, 2009.
39. Zainud-Deen, S. H., E. El-Deen, M. S. Ibrahim, K. H. Awadalla, and A. Z. Botros, "Electromagnetic scattering using gpu-based finite difference frequency domain method," *Progress In Electromagnetics Research Letters*, Vol. 6, 157–164, 2009.
40. Zheng, G., B.-Z. Wang, H. Li, X.-F. Liu, and S. Ding, "Analysis of finite periodic dielectric gratings by the finite-difference frequency-domain method with the sub-entire-domain basis functions and wavelets," *Progress In Electromagnetics Research*, Vol. 99, 453–463, 2009.
41. Chang, H.-W., Y.-H. Wu, and W.-C. Cheng, "Hybrid FD-FD analysis of crossing waveguides exploiting plus and cross symmetry," *Progress In Electromagnetics Research*, Vol. 103, 217–240, 2010.
42. Wu, T.-L. and H.-W. Chang, "Guiding mode expansion of a TE and TM transverse-mode integral equation for dielectric slab waveguides with an abrupt termination," *J. Opt. Soc. Amer. A*, Vol. 18, 2823–2832, 2001.
43. Bock, P. J., P. Cheben, J. H. Schmid, J. Lapointe, A. Delâge, D.-X. Xu, S. Janz, A. Densmore, and T. J. Hall, "Subwavelength grating crossings for silicon wire waveguides," *Optics Express*, Vol. 18, No. 15, 16146–16155, 2010.